Loading-rate dependent shear failure model of geo-material and its application to the ballistic testing of granite targets

Gyeongjo Min*, Sewook Oh*, Yohan Yoo**, Leeju Park**,
Hyungseop Sin***, Yongwon Ju**, and Sangho Cho*†

*Department of Mineral Resources & Energy Engineering, Jeonbuk National University, 567 Baekje-daero, Deokjin-gu, Jeonju-si, Jeollabukdo, REPUBLIC OF KOREA
 Phone: +82-63-270-4636
†Corresponding author: chosh@jbnu.ac.kr

**Agency for Defense Development, 160, Bugyuseong-daero 488beon-gil, Yuseong-gu, Daejeon, REPUBLIC OF KOREA

***Department of Mechanical Design Engineering, Andong National University, REPUBLIC OF KOREA

Abstract

Penetration and perforation performance of the rock targets by hard projectiles is suitable for understanding the ballistic behavior of the strategic and important structures such as protective structures, bunkers, ammunition stores, and nuclear power plants that are sensitive to missile impacts. In this study, ballistic penetration tests and numerical simulations were performed to examine the behavior of geo-material targets against hard projectile impacts. The granitic rock plates were used as target materials, and the projectiles were made of hardened 4340 steel. A loading−rate dependent shear failure model was suggested based on experimental data and implemented into LS-DYNA using a user-material subroutine. The ballistic test results were used to validate the suggested model. The numerical ballistic data simulated experimental behaviors relatively well.

1. Introduction

The ballistic performance of geo-material is appropriate to understand the damage behavior of protective structures, bunkers, ammunition stores, and nuclear containments against missile impact[1]. In general, there are several methods (i.e., empirical methods, analytical method, and numerical analysis) for investigating and predicting the ballistic performance of geo-material targets subjected to projectile impact. Several empirical and analytical methods provided as a solution for a problem involving a projectile impacting a geo-material target with proper experimental validation and assumptions. To determine the depth of penetration into rock, Bernard and Creighton[2] proposed the empirical model, which considers the quality of rock impacted by an ogive-nosed and conical-nosed projectile. Also, Seah et al.[3] developed a three-stage analytical model to predict the perforation of target plates by hard projectile based on the ballistic perforation experiments. However, the empirical and analytical methods cannot provide a detailed analysis of stresses and deformation occurring during the rock target penetration and perforation. Hence, to acquire a more comprehensive and reliable solution, a numerical approach should be applied. Moreover, to acquire a reliable numerical simulation result, the application of a valid constitutive model of geo-material is necessary. Also, as the projectile penetrates the rock target, the projectile is confined by surrounding target material where the

extremely high pressure, high strain rate, and large deformation are induced[4]. Hence, the constitutive model of the geo-material should deal with the aforementioned conditions to simulate rock penetration of the projectile. Meanwhile, several constitutive models have been applied for geo-material, which include Johnson-Holmquist ceramic (JH-2) model[5] and Riedel-Hiermaier-Thoma (RHT) concrete model[6] that describe the effect of strain-rate and high pressure on compressive and tensile strength. But the rock penetration of the projectile, which is launched with few hundred m/s, is more dependent on shear strength, which is dependent on confining pressure, than tensile strength and compressibility[7]. Furthermore, it is hard to use the model based on hydrostatic pressure data at Hugoniot state, which is difficult to obtain[8].

In this study, the ballistic penetration tests of granitic rock plate targets which have different thicknesses were performed using a compressed gas gun system. The loading-rate dependent Mohr-Coulomb (RDMC) model based on the dynamic shear failure tests with the confined condition is developed and implemented into LS-DYNA with shear and tensile damage criterion. The numerical simulation model was chosen for validation of the dynamic shear failure model as the rock target, which subjected to the projectile impact. And simulation results were also compared with the experiment result.

2. Ballistic testing for the granite target subjected to projectile impact
2.1 Compressed gas gun system

A compressed gas gun system, as shown in Figure 1(a), was utilized to perform the ballistic penetration tests for granite targets. The main components of the system consist of a 10 MPa pressure gas tank, which has a solenoid firing system, a 2 m-long barrel with a 10 mm-diameter hole, and a chamber for protection. A steel projectile is devised with 20 g-mass and 10 mm-diameter steel material. The initial impact velocity of the projectile was measured by two sets of the photodiode and laser diodes, which were mounted in the gun barrel and signal data acquisition system, as shown in Figure 1(b). The residual velocity of the projectile after penetrating the target was measured by a high-speed camera which shots flying target after penetration through the protective

glass of the chamber. During each test, the granite block was fixed into specially designed steel mass and steel frame with bolting, as shown in Figure 1(b), to satisfy confined condition when the projectile impacts the target center. The steel mass and steel frame were available to satisfy confined condition by preventing deflection around the target center.

2.2 Projectiles and targets

The projectiles were manufactured from 4340 steel, which has the density of $7460 \, \mathrm{kg \cdot m^{-3}}$, Young's modulus of 209.5 GPa and Poisson's ratio of 0.28. Detailed dimensions and photographs of the steel projectile are given in Figure 2(a).

The granitic targets were prepared to square-shaped granite plate targets with a dimension of $200 \, \mathrm{mm} \times 200 \, \mathrm{mm}$ and thickness of $10-20 \, \mathrm{mm}$ as shown in Figure 2(b). The physical and mechanical properties of the granite rock are listed in Table 1.
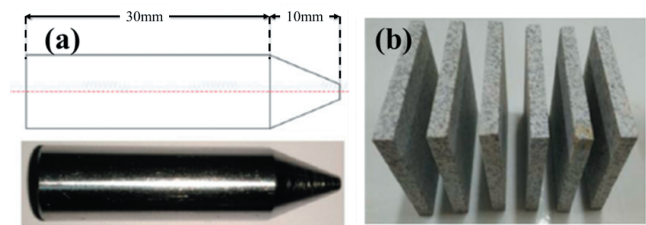

Figure 2 The photograph of (a) the steel (STEEL4340) projectile and (b) granitic rock targets.

Table 1 Physical and mechanical properties of the granitic rock.

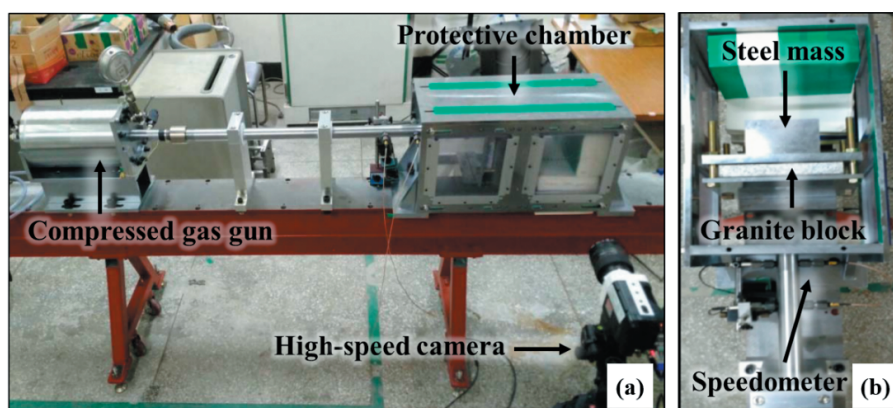| Material property	Unit	Value
Density	$\mathrm{kg \cdot m^{-3}}$	2604
Young's modulus	GPa	46
Poisson's ratio	−	0.21
Uniaxial compressive strength	MPa	202
Tensile strength	MPa	10
Cohesion	MPa	26
Internal friction angle	Degree	58.1
Material constant (A)	−	0.5010

Figure 1 Compressed gas gun system for ballistic testing of the granite targets.

2.3 Ballistic testing for granite targets

The initial impact velocity of the projectile was varied from $100 \, \text{m·s}^{-1}$ to $350 \, \text{m·s}^{-1}$ by the controller valve of the firing system to assess the ballistic resistance of the granitic rock targets. For every experiment, the initial and residual velocities of the projectiles were measured and captured by the high-speed camera, as shown in Figure 3 (a). The relationship between the residual velocity and initial velocity, which plotted with different thicknesses in Figure 3 (b), showed a typical tendency of the metal penetration tests. The residual velocity suddenly increased at an initial velocity and reached the linear line. Figure 4 presents the front and the rear side view of the granite targets with different thicknesses. The diameter of the penetration hole was almost equivalent, but the size of the crater which was shown on the rear side increased with increasing thickness of the targets.

3. Numerical analysis approaches

Finite element (FE) models were adopted to simulate the granite targets with different thicknesses subjected to high-velocity projectile impact. A loading-rate dependent shear failure criterion, based on dynamic shear tests under confined conditions, was applied in the constitutive model and implemented into multi-physical software LS-DYNA with application user-defined material subroutine (UMAT). The UMAT is available to independently develop the constitutive model of numerical simulation, which is not interfaced in the LS-DYNA[8]. Furthermore, Slip-weakening and Taylor-Chen-Kuszmaul (TCK) damage criterion were also applied as an element erosion criterion.

3.1 Loading-rate dependent Mohr-Coulomb (RDMC) criterion

The previous study[10] proposed a dynamic shear punch test method to obtain the shear strength of the granitic rock with different constant confining pressure and loading rates. The dynamic shear punch tests revealed that the shear strength increased with increasing confining pressure and significantly increases with loading-rate increments.
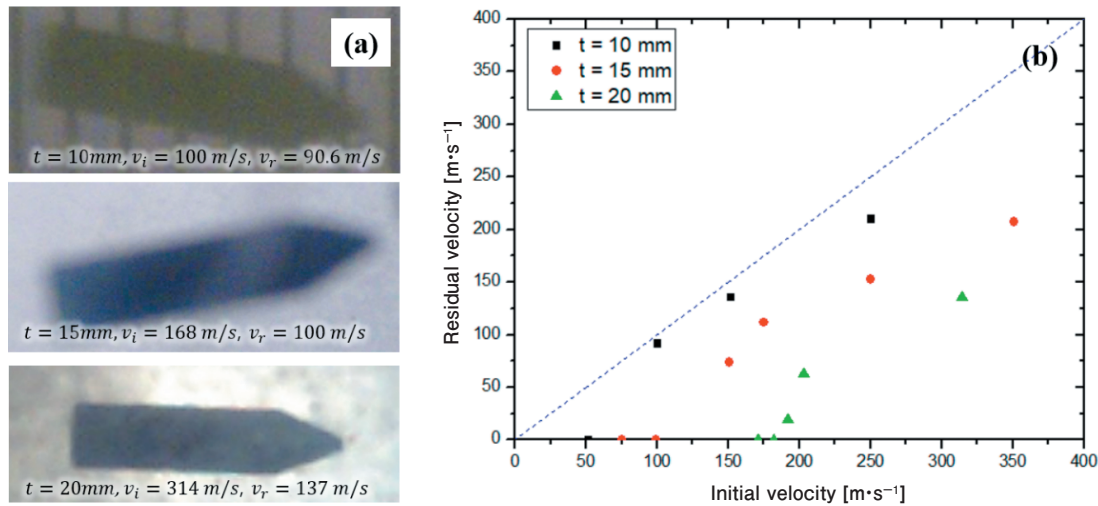

Figure 3   Result of ballistic test for granite target (a) high-speed camera images and (b) plot of residual velocity − initial velocity of different thickness of granite target.
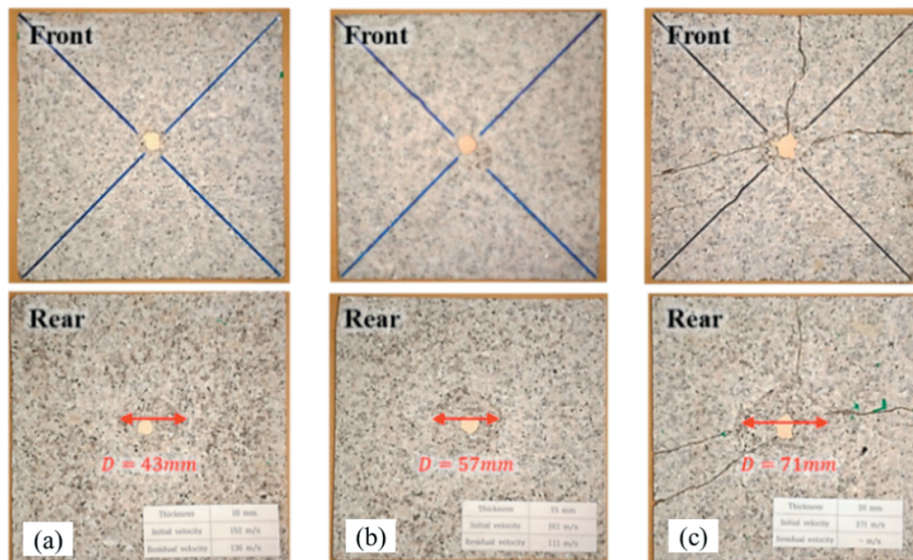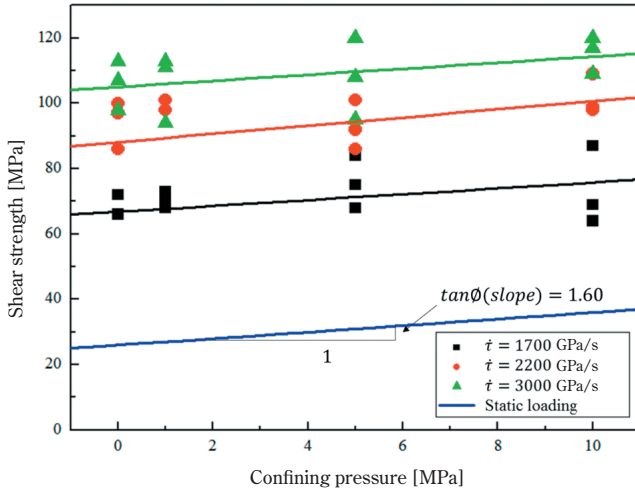

Figure 4   Frontal and backside view of the tested granite targets when (a) $t = 10$ mm, (b) $t = 15$ mm and (c) $t = 20$ mm.

Figure 5   Dynamic shear strength of the Granite as a function of confining pressure under loading-rate.

Figure 6   Graphical representation of linear slip-weakening.

Based on the conventional Mohr-Coulomb formation[11], the behavior of shear strength can be explained as the cohesion (intercept) increased with loading rate increment, whereas the internal friction angle (slope) is almost equivalent to every different loading rate condition as shown in Figure 5.

Therefore, the obtained shear strength data were rearranged as a function of constant confining pressure and loading rates based on Mohr-Coulomb failure criterion as

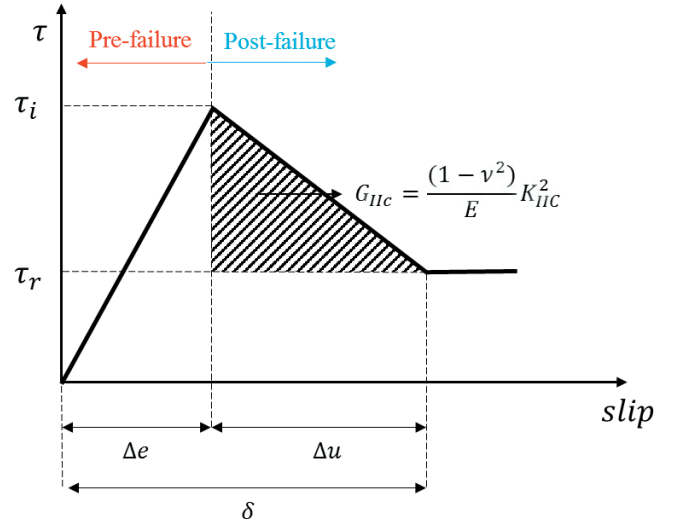$$\tau = c \left(1 + A \ \ln \frac{\dot{\tau}}{\dot{\tau}_0} \right) + \sigma_n \tan \phi \tag{1}$$

Where τ is shear strength, $\dot{\tau}$ is loading-rate, $\dot{\tau}_0$ is reference loading-rate, σ_n is confining pressure, c is cohesion, ϕ is internal friction angle, and A is coefficient of loading-rate dependent. In this study, reference loading-rate 19.01 GPa·s^{-1} was used.

The RDMC criterion was applied to the constitutive model, which modifies the stress of material as its shear stress exceeds or satisfy the shear failure criterion.

3.2 Element erosion criterion

As the projectile penetrates into rock target in the numerical simulation, the element erosion (deletion) criteria should be applied for dealing with a large deformation, which leads to significant numerical instability in continuum-based FEM application. In this study, two erosion criteria, including slip-weakening (shear erosion) and Taylor-Chen-Kuszmaul (TCK) damage (tensile erosion) has been also applied to UMAT in LS-DYNA.

The slip-weakening model, which is implemented as shear erosion criterion, has been adapted to model the mechanics of geo-materials, where the shear strength degrades with slip displacement as shown in Figure 6[12),13]. The slip-weakening model has a peak value of τ_i at the beginning of the slip weakening and the shear strength decreases until it stabilizes to a residual strength τ_r. Assumed that if the total shear displacement δ of any element exceeds the summation of displacement of pre-

failure Δe and post-failure Δu, the erosion of the element occurs. The pre-failure displacement Δe can be defined as the following equation;

$$\Delta e = \frac{\tau L}{G} \tag{2}$$

Where τ is the shear stress, L is the average mesh size of the model, and G is the shear modulus. Also, the post-failure displacement Δu can be written as

$$\Delta u = \frac{G_{IIC}}{0.5 \, (\tau_i - \tau_r)} \tag{3}$$

In this study, fracture energy G_{IIC} was 1.12 kJ·m^{-2} and the average mesh size L was 0.001 m. And also, when any element reaches the shear displacement (δ), the elements are deleted.

According to the TCK damage model, which is adopted as a tensile erosion criterion in this study, any impact-induced tensile damage should cause the degradation of the material stiffness and can be defined as the following equation[14]:

$$D = \frac{16}{9} \frac{(1 - \overline{v}^2)}{(1 - 2\overline{v})} C_d \tag{4}$$

Where D $(0 \le D \le 1)$ is tensile damage, $\overline{v}$ is a degraded constant of Poisson's ratio, and C_d is a crack density. The crack density C_d can be calculated as the following equation:

$$C_d = \frac{5}{2} k \ (\varepsilon_v)^m \left(\frac{K_{IC}}{\rho C \dot{\varepsilon}_{v \, \max}} \right)^2 \tag{5}$$

Here, k and m are material constants, that can be determined from the relationship between the strain-rate and tensile fracture strength. ε_v is a volumetric strain, K_{IC} is the mode I fracture toughness of the material, ρ is the mass density, C is the elastic wave velocity, and $\dot{\varepsilon}_{v \, \max}$ is the maximum volumetric strain-rate. Also, the degraded constant of Poisson's ratio $\overline{v}$ can be calculated as the following equation:

Table 2   Input parameters of the granitic rock targets for the tensile damage criterion.

Material property	Unit	Value
Material constant (k)	m^{-3}	1.7×1034
Material constant (m)		8.0
Fracture toughness (K_{Ic})	MPa·m$^{-1/2}$	1.12
Proportionality constant (β)		0.5
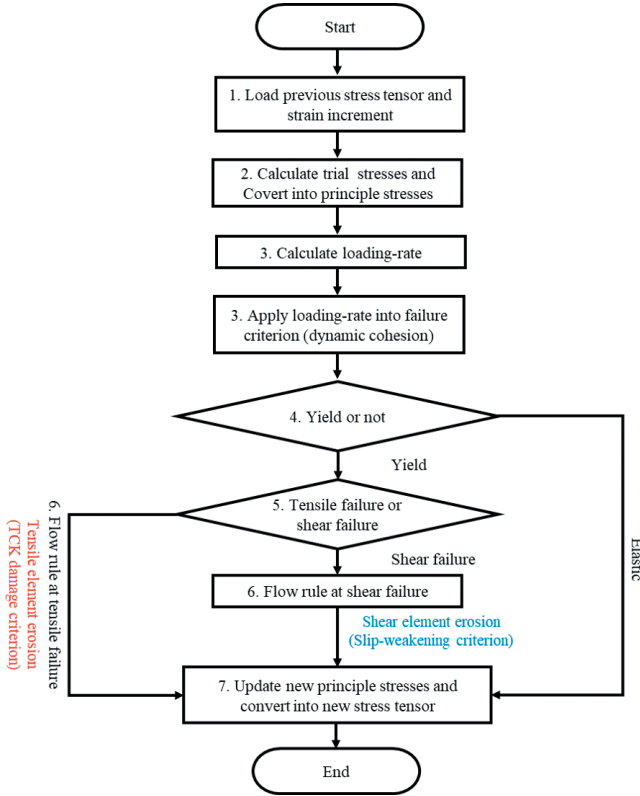
**Figure 7**   The flowchart of the constitutive model including the RDMC failure criterion applied UMAT in LS-DYNA[15].

$$\overline{v} = v \exp\left(-\frac{16}{9}\beta C_d\right) \qquad (6)$$

Where v is the original Poisson's ratio and β is the proportionality constant ($0 \leq \beta \leq 1$). In the present study, when the tensile damage value (D) of any element reaches 1, the elements are deleted. The material parameters of the granite target for calculating the tensile damage are summarized in Table 2.

Figure 7 presents the UMAT flowchart of the constitutive model with the RDMC criterion, including tensile damage and slip weakening as the element erosion criterion.

3.3 Configuration and boundary condition of ballistic test simulation

The FE models were generated using the pre-processing software LS-Prepost, which was applied in the LS-DYNA. Figure 8 presents the layout of finite elements for analyzing the ballistic tests of the granitic rock targets. The projectile was modeled as an elastic body in LS-DYNA because damages of the tested projectiles were
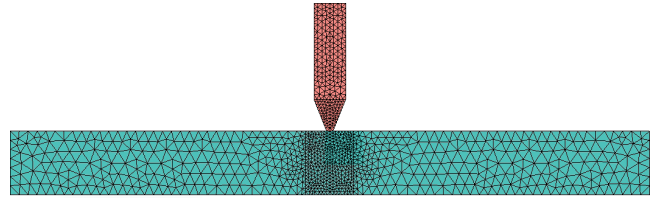
Figure 8   Finite element layout for analyzing the projectile ballistic test of granite target.

invisible. The initial impact velocity of the projectile was increased from $100\,\text{m·s}^{-1}$ to $350\,\text{m·s}^{-1}$ in LS-DYNA simulation. The FE models of the granitic rock targets were assigned as the constitutive model including the RDMC and element erosion criterion using LS-DYNA UMAT. Input parameters of the granite targets are listed in Table 1.

3.4 Result of numerical simulation

Figure 9(a) shows the numerical penetration process of the RDMC granitic rock model when initial impact velocity = 200 m·s^{-1} and the thickness of the target model = 15 mm. Figure 9(b) plotted the numerical and experimental residual velocities of the projectiles as the function of the initial velocity. The numerical simulation results show that similar behaviors with experimental results where the residual velocity suddenly increased at the velocity of the ballistic limit and after reached the linear line. It is conceivable that the simulation result shows good agreement with experiment data around the ballistic limit as well as the velocities of the ballistic limit were coincident with the experimental data. However, after the residual velocity reaches the linear line, the penetration performance shows a little more exaggerated than the experimental results.

It is noteworthy that the suggested RDMC combined with the tensile/shear erosion criterion reproduced the experimental ballistic penetrations of the granitic rock targets without using the element erosion function supplied in LS-DYNA. However, in high-velocities of the projectile over $250\,\text{m·s}^{-1}$, additional calibration and further study for high-velocity impact are needed for exact ballistic performance estimation.

4. Discussions

Many studies adapted JH-2 constitutive models to describe the effects of strain-rate and high pressure on compressive and tensile strength for simulating geo-material targets subjected to hard projectile impact. It is worth noting that the suggested RDMC model can be explained with the JH-2 model. The material constants of JH-2 for the intact granite ($D = 0$) were analyzed and found to be $A = 1.67$, $N = 0.49$ and $C = 0.0024$. Thus, the equation of JH-2 ($D = 0$) can be written as:

$$\sigma_i^* = 1.67(P^* + T^*)^{0.49}(1 + 0.0024\ln\dot{\varepsilon}^*) \qquad (7)$$

If the value of N is approximated as 0.5, the above equation for $\dot{\varepsilon} = 178.94\ s^{-1}$ can be simplified[16] as the following equation:
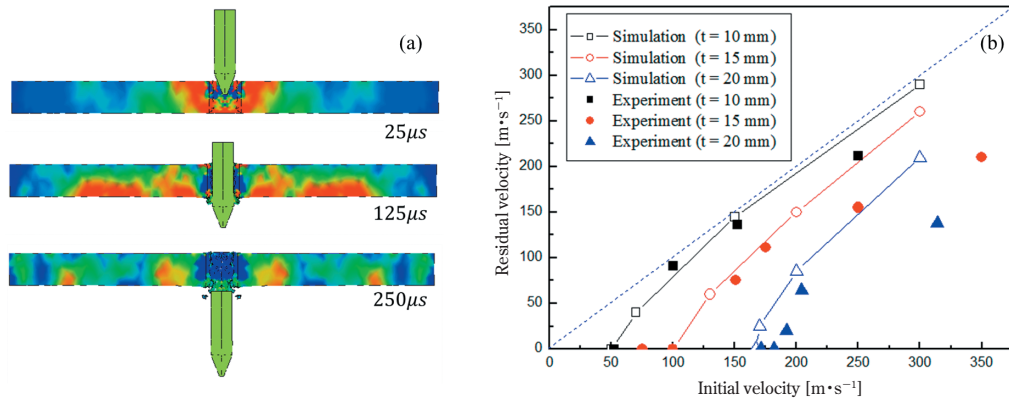
Figure 9 Numerical penetration tests using RDMC model (a) an example of perforation processes of granite targets and (b) comparison of the numerical tests with the experimental data.

$$\tau = 0.76P + 49.94 \qquad (8)$$

A comparison of the RDMC model ($\tau = 1.6P + 68$) and Equation (8) reveals that they show very similar form and values. It means that the failure behavior of geo-material can be sufficiently described by the RDMC model as the substitution of the JH-2 model.

5. Conclusion

In this study, the compressed gas gun system was adopted to assess the penetration performance of a granite target subjected to steel projectile impact with $100 - 350 \, \mathrm{m \cdot s^{-1}}$ impact velocity. The ballistic penetration test results showed that the residual velocity dramatically increased at the ballistic limit velocity, which initially perforated, and then linearly increased with initial impact velocity increment. The relationship between residual velocity and initial velocity was employed to compare experimental results with numerical simulation. The numerical simulation of the ballistic penetration of the granite target was performed with the RDMC model. The simulation results presented that the RDMC model can simulate relatively well the penetration process of granite targets as well as the ballistic limit and residual velocity with relative precision. However, at over impact velocities over $250 \, \mathrm{m \cdot s^{-1}}$, the additional calibration and further studies for the high-velocity impact are needed for precise estimation of the ballistic performance. Moreover, it is revealed that the RDMC model can be replaced with the JH-2 model for describing the failure behavior of geo-material, sufficiently.

Acknowledgments

References

1) A. Rajput and M. A. Iqbal, Materials & Design, 114, 459–474 (2017).
2) R. S. Bernard and D. C. Creighton, Projectile penetration in soil and rock: Analysis for non-normal impact (Report WES /TR/SL-79-1). New Mexico: Army Engineer Waterways Experiment Station (1979).
3) C. C. Seah, T. Borvik, S. Remseth, and T–C. Pan, "Penetration and perforation of rock targets by hard projectiles", 7, 143–162, Advances in Rock Dynamics and Applications, CRC Press (2011).
4) Q. Fang and W. Hao, "Concrete structures under projectile impact." Concrete Structures Under Projectile Impact. Springer, Singapore (2017).
5) G. R. Johnson and J. H. Tim, "An improved computational constitutive model for brittle materials." AIP conference proceedings. Vol. 309. No. 1. AIP (1994).
6) W. Riedel, K. Thoma, S. Hiermaier, and E. Schmolinske, Proceedings of the 9th International Symposium on the Effects of Munitions with Structures. Vol. 315. Berlin-Strausberg Germany (1999).
7) F. E. Heuze, Int. J. Rock Mech. Min. Sci. abst. Vol. 27. No. 1. Pergamon (1990).
8) T. J. Holmquist, G. R. Johnson, C. M. Lopatin, D. E. Grad, and E. S. Her Jr, High strain rate properties and constitutive modeling of glass. No. SAND-95-0379C; CONF-950537-2. Sandia National Labs., Albuquerque, NM (United States) (1995).
9) T. Erhart, LS-DYNA Forum (2010).
10) G. J. Min, S. W. Oh, M. S. Kim, J. J. Yoon S. H. Cho, and L. J. pa,Rock Dynamics: From Research to Engineering: Proceedings of the 2nd International Conference on Rock Dynamics and Applications. CRC Press (2016).
11) C. A. Coulomb, "Essai sur une application des rèles des maximis et minimis a quelques problems de statique." Memoires Acad. Royale des Sciences 7 (1776).
12) Y. Ida, J. Geophys. Res. 77.20 3796–3805 (1972).
13) A. C. Palmer and R. R. James, Proceedings of the Royal Society of London. A. Mathematical and Physical Sciences 332.1591 527–548 (1973).
14) B. Budiansky and J. O'. Richard, Int. J. Solids Struct. 12.2 81 –97 (1976).
15) G. Min, S. Oh, S. Park, S. Cho, Y. You, and L. Park, 2019 Rock Dynamics Summit: Proceedings of the 2019 Rock Dynamics Summit (RDS 2019), May 7–11, 2019, Okinawa, Japan (2019): 125.
16) W. Chen, Dynamic failure behavior of ceramics under multiaxial compression., Ph. D. Diss., California Institute of Technology (1995).